Transverse momentum distributions of valence quarks in light and heavy vector mesons

Chao Shi,[1,*] Jicheng Li,[1] Ming Li,[1] Xurong Chen,[2,3] and Wenbao Jia[1]

[1]Department of Nuclear Science and Technology, Nanjing University of Aeronautics and Astronautics, Nanjing 210016, China

[2]Institute of Modern Physics, Chinese Academy of Sciences, Lanzhou 730000, China

[3]Guangdong Provincial Key Laboratory of Nuclear Science, Institute of Quantum Matter, South China Normal University, Guangzhou 510006, China

(Received 6 May 2022; accepted 13 July 2022; published 28 July 2022)

We study the leading-twist time-reversal even transverse momentum-dependent parton distribution functions (TMDs) of light and heavy vector mesons, i.e., the ρ, J/ψ and Υ. We employ the leading Fock-state light front wave functions (LF-LFWFs) of ρ and J/ψ from our recent study, and supplement with Υ's LF-LFWFs. These LF-LFWFs are extracted from dynamically solved Bethe-Salpeter wave functions. The vector meson TMDs are then studied with the light front overlap representation at leading Fock-state. All the obtained TMDs are nonvanishing and evolve with current quark mass, in particular the tensor polarized TMDs f_{1LT} and f_{1TT} which undergo a sign flip. The ρ TMDs are compared with other model studies and agreement is found, aside from f_{1LT} and f_{1TT}. Finally, the collinear PDFs of vector mesons are studied. The ρ's valence PDFs $f_{1,v}(x)$ and $g_{1L,v}(x)$ are evolved to the scale of 2.4 GeV, with their first three moments compared to the lattice QCD prediction. The qualitative behavior of tensor polarized PDF $f_{1LL}(x)$ in ρ at large x is also discussed.

DOI: 10.1103/PhysRevD.106.014026

I. INTRODUCTION

Multidimensional imaging of hadrons has excited a lot of interest for the last several decades. The transverse momentum-dependent parton distributions (TMDs), in this connection, provide an important extension to the one-dimensinal parton distribution functions (PDFs) by incorporating the transverse motion of the partons and spin-orbit correlations [1–4]. The TMDs of the pion and nucleon which are spin-0 and spin-1/2, respectively, have thus received extensive studies from phenomenological models [5–10] and lattice QCD [11–14]. Experimentally, they can be studied with the Drell-Yan or semi-inclusive deep-inelastic scattering (SIDIS) processes [15–20].

Meanwhile, the parton distributions of spin-1 particle has also been studied in the literature. Starting with the one-dimensional case, a new PDF, i.e., the tensor polarized PDF $b_1^q(x)$ (the superscript q refers to quark), emerges in spin-1 target at leading twist [21]. It is interpreted as the difference between unpolarized quark distribution function in $\Lambda = 0$ and $|\Lambda| = 1$ targets, where the Λ is the helicity. The sum rule $\int dx[b_1^q(x) - b_1^{\bar{q}}(x)] = 0$ thus holds, as the total valence quark in $\Lambda = 0$ and $|\Lambda| = 1$ targets should be equal [22,23]. The tensor structure function $b_1(x)$ of the deuteron is then measured by HERMES Collaboration, and found to be nonzero at low $x(x < 0.1)$ [24]. In the three-dimensional case, the TMDs and TMD fragmentation functions of spin-1 target are introduced [25]. The Soffer bound is then generalized to the case of spin-1 and positivity bounds on TMDs and TMD FFs are obtained [26]. While no experimental measurement on spin-1 TMDs is available at present, theoretical study can provide insight into the 3D structure of spin-1 particles in the momentum space. The ρ meson TMDs have thus been studied with the Nambu–Jona-Lasinio (NJL) model [27] and light front models [28], and some photon TMDs are studied with the basis light front quantization (BLFQ) approach [29].

In this work, we study the TMDs of both light and heavy vector mesons, i.e., ρ, J/ψ and Υ. Among them, the ρ meson is constituted from light quarks, with its mass mostly generated by the dynamical chiral symmetry breaking of QCD at low energy [30,31]. The J/ψ and Υ, on the other hand, gain their masses mostly from the current quark mass generated by the Higgs mechanism. Meanwhile, the parton motion within ρ is highly relativistic, while in the J/ψ and Υ it is much slower and nonrelativistic, in particular in the Υ. By studying the TMDs of light and heavy vector mesons simultaneously, one can investigate the TMDs in both the relativistic and nonrelativistic limit, as well as the dynamical chiral symmetry breaking effect in shaping them.

*cshi@nuaa.edu.cn

There are generally two approaches to calculate the vector meson TMDs, i.e., the covariant approach and the light front approach. The former calculates the covariant Feynman diagrams, such as in [27], and the latter resorts to overlap representations in the light front QCD. Both approaches have their own advantages. For instance, the covariant approach could circumvent the direct calculation of higher Fock-state light front wave functions (LFWFs), which has been a hard task in practice. On the other hand, the light front overlap representation approach gives a direct parton picture in terms of the LFWFs. The parton and parent hadron polarization can be read off explicitly, along with the orbital angular momentum (OAM) transfer among them [7]. Meanwhile, positivity bounds can be conveniently derived in the light front approach, and hence automatically satisfied in light front model studies [26,32]. In this work, we utilize the light front overlap representation at leading Fock-state approximation and study the vector meson TMDs at leading twist.

The LF-LFWFs of vector meson employed in this study are extracted from their covariant Bethe-Salpeter (BS) wave functions. The basic idea is to project the BS wave functions on to the light front [33–35]. It has been demonstrated with the pseudoscalar mesons [10,36,37] and then generalized to the case of vector mesons [38]. Based on the dynamically solved BS wave functions, which accumulated lots of success in hadron study within the Dyson-Schwinger equations (DSEs) formalism [39–45], the parton distribution amplitude [46–48], generalized parton distributions (GPDs) and TMDs of pseudoscalar mesons [49,50] are further studied. Exclusive process is also studied, e.g., without introducing any new parameters, the ρ and J/ψ LF-LFWFs are put into the color dipole model study of diffractive vector meson productions in $e-p$ collisons, and agreement is found with data from HERA [38]. In this work, we extend our study to vector meson TMDs. Since the light and heavy vector mesons can be studied consistently in the DSEs, we also include the Υ meson. As we will show, the Υ is well dominated by the leading Fock-states, and therefore provides a benchmark for TMDs in the nonrelativistic limit, which has not been reported in the literature before.

This paper is organized as follows. In Sec. II we introduce the BSE-based LF-LFWFs of vector mesons and supplement with the Υ case. We then recapitulate the definition of vector meson TMDs and their overlap representation in Sec. III. The TMDs of heavy and light vector mesons are reported in Sec. IV, where comparison will be made with other model studies. The collinear PDFs will also be studied. Finally, we summarize in Sec. V.

II. VECTOR MESON LF-LFWFS FROM BETHE-SALPETER WAVE FUNCTIONS

The extraction of vector meson LF-LFWFs from BS wave functions has been introduced with detail in [38]. Here, we recapitulate the formalism. In light front QCD, the leading Fock-state expansion of a vector meson reads

$$|M\rangle^{\Lambda} = \sum_{\lambda,\lambda'} \int \frac{d^2\boldsymbol{k}_T}{(2\pi)^3} \frac{dx}{2\sqrt{x\bar{x}}} \frac{\delta_{ij}}{\sqrt{3}} \times \Phi^{\Lambda}_{\lambda,\lambda'}(x,\boldsymbol{k}_T) b^{\dagger}_{f,\lambda,i}(x,\boldsymbol{k}_T) d^{\dagger}_{g,\lambda',j}(\bar{x},\bar{\boldsymbol{k}}_T)|0\rangle. \quad (1)$$

The $\Phi^{\Lambda}_{\lambda,\lambda'}$ is the LF-LFWF of meson with helicity Λ and quark (antiquark) with spin λ (λ'). The $\Lambda = 0, \pm 1$ and $\lambda = \uparrow$ or $\downarrow$, which will be denoted as $\uparrow = +$ and $\downarrow = -$ for abbreviation in the following. The i and j are color indices. The $\boldsymbol{k}_T = (k^x, k^y)$ is the transverse momentum of the quark with flavor f, and $\bar{\boldsymbol{k}}_T = -\boldsymbol{k}_T$ for antiquark with flavor g. The longitudinal momentum fraction carried by quark is $x = k^+/P^+$, with $\bar{x} = 1 - x$ for antiquark. The light cone four-vector of this paper is defined as $A^{\pm} = \frac{1}{\sqrt{2}}(A^0 \pm A^3)$ and $\boldsymbol{A}_T = (A^1, A^2)$.

The vector meson LF-LFWFs can be extracted from their covariant Bethe-Salpeter wave functions with [38]

$$\Phi^{\Lambda}_{\lambda,\lambda'}(x,\boldsymbol{k}_T) = -\frac{1}{2\sqrt{3}} \int \frac{dk^- dk^+}{2\pi} \delta(xP^+ - k^+) \times \mathrm{Tr}[\Gamma_{\lambda,\lambda'}\gamma^+ \chi^M(k,P) \cdot \epsilon_{\Lambda}(P)]. \quad (2)$$

The $\chi^M_{\mu}(k,P)$ is the BS wave function in the momentum space and the $\epsilon_{\Lambda}(P)$ is the meson polarization vector. The $\Gamma_{\pm,\mp} = I \pm \gamma_5$ and $\Gamma_{\pm,\pm} = \mp(\gamma^1 \mp i\gamma^2)$ project out corresponding quark-antiquark helicity configurations.[1] The trace is taken over Dirac, color, and flavor spaces. An implicit color factor δ_{ij} is associated with $\Gamma_{\lambda,\lambda'}$. The flavor index yields unity as we will consider ρ^+ ($u\bar{d}$), $J/\psi(c\bar{c})$, and $\Upsilon(b\bar{b})$ in this work.

The $\Phi^{\Lambda}_{\lambda,\lambda'}(x,\boldsymbol{k}_T)$'s can be further expressed with six independent scalar amplitudes $\psi(x,\boldsymbol{k}_T^2)$'s [51,52], i.e.,

$$\Phi^0_{\pm,\mp} = \psi^0_{(1)}, \qquad \Phi^0_{\pm,\pm} = \pm k_T^{(\mp)} \psi^0_{(2)}, \quad (3)$$

$$\Phi^{\pm 1}_{\pm,\pm} = \psi^1_{(1)}, \qquad \Phi^{\pm 1}_{\pm,\mp} = \pm k_T^{(\pm)} \psi^1_{(2)},$$
$$\Phi^{\pm 1}_{\mp,\pm} = \pm k_T^{(\pm)} \psi^1_{(3)}, \qquad \Phi^{\pm 1}_{\mp,\mp} = (k_T^{(\pm)})^2 \psi^1_{(4)}, \quad (4)$$

with $k_T^{(\pm)} = k^x \pm i k^y$. For the unflavored vector meson (J/ψ or Υ) that has charge parity, further constraints can be found [38]

$$\psi^{\Lambda}_{(i)}(x,\boldsymbol{k}_T^2) = \psi^{\Lambda}_{(i)}(1-x,\boldsymbol{k}_T^2), \quad (5)$$

except

[1] $\Gamma_{\pm,\mp} = I \pm \gamma_5$ refers to $\Gamma_{+,-} = I + \gamma_5$ and $\Gamma_{-,+} = I - \gamma_5$, which is by taking the sign in the same row simultaneously. This notation applies throughout this paper.

TABLE I. Calculated masses and decay constants of pseudoscalar and vector mesons based on model setup of [38,54]. All units are in GeV. The second and fourth row are based on PDG data [55], with lattice QCD results explicitly indicated by references.

	π	η_c	η_b	ρ	J/ψ	Υ
m	0.131	2.92	9.40	0.72	3.09	9.48
$m_{\rm exp}$	0.138	2.98	9.39	0.78	3.10	9.46
f	0.090	0.270	0.476	0.141	0.300	0.460
$f_{\rm exp/lQCD}$	0.092	0.279 [56]	0.489 [57]	0.156	0.294	0.459 [58]

$$\psi^1_{(2)}(x,\boldsymbol{k}_T^2) = -\psi^1_{(3)}(1-x,\boldsymbol{k}_T^2). \tag{6}$$

This reduces the number of independent scalar amplitudes to five. Note that the LF-LFWFs can also be classified by their quark-antiquark OAM projection along the z-axis, which is denoted by l_z [52]. The angular-momentum conservation in the z-direction enforces $\Lambda = \lambda + \lambda' + l_z$. Based on Eqs. (3) and (4) the l_z can be 0, ±1, and ±2, which are s-, p-, and d-wave LF-LFWFs, respectively.

The ρ^0 and J/ψ LF-LFWFs have been presented in [38]. They are based on BS wave functions under rainbow-ladder truncation. In this case, one does not discriminate between ρ^0 and $\rho^\pm$ BS wave functions, so the ρ^0 LF-LFWFs applies to ρ^+ as well. In this work, we supplement with the Υ meson LF-LFWFs, which is obtained in the same way as J/ψ. Since Υ is significantly heavier than J/ψ, it could help zoom into the nonrelativistic limit. The three-dimensional plots of LF-LFWFs for ρ^+, J/ψ and Υ can be found in the Appendix.

The interaction model and parameters [31,53] are required at the step of solving the quark gap equation and vector-meson BS equation. The setup in this work follows exactly that in [38] for ρ^+ and J/ψ. The bottom quark was incorporated later in [54] for the study of η_b. Aside from the interaction model, the current quark mass we employed is $m_{u/d} = 5$ MeV, $m_c(m_c) = 1.33$ GeV, and $m_b(m_b) = 4.30$ GeV. The calculated meson mass and leptonic decay constants are listed in Table. I. Note that the vector meson leptonic decay constants can be calculated using the BS wave function $\chi_\mu(q;P)$ with [31]

$$f_V m_V = \int^\Lambda \frac{dq^4}{(2\pi)^4} \mathrm{Tr}[\gamma\cdot\chi(q;P)], \tag{7}$$

and meanwhile reproduced using the LF-LFWF $\phi^{\Lambda=0}_{\pm,\mp}$ with

$$f_V = \sqrt{6}\int_0^1 dx \int^\Lambda \frac{d^2\boldsymbol{k}_T}{(2\pi)^3}\phi^{\Lambda=0}_{\pm,\mp}(x,\boldsymbol{k}_T^2), \tag{8}$$

as Eq. (7) and Eq. (8) are actually equivalent given Eq. (2).

III. DEFINITION AND OVERLAP REPRESENTATION OF VECTOR MESON TMDS

The TMDs of spin-1 hadrons are defined in connection with the transverse momentum-dependent quark correlation function

$$\Theta^{(\Lambda)s}_{\beta\alpha}(x,\boldsymbol{k}_T) = \int \frac{dz^- d^2\boldsymbol{z}_T}{(2\pi)^3} e^{i(xP^+z^- - \boldsymbol{k}_T\cdot\boldsymbol{z}_T)} \times {}_S\langle P,\Lambda|\bar\psi_\alpha(0)\psi_\beta(z^-,\boldsymbol{z}_T)|P,\Lambda\rangle_S. \tag{9}$$

Here the P is the four-momentum of the hadron with $\boldsymbol{P}_T = 0$, and xP^+ and $\boldsymbol{k}_T$ are the longitudinal and transverse momentum carried by the parton. The $\boldsymbol{S} = (\boldsymbol{S}_T, S_L)$ is the spin quantization axis, and $\Lambda = 0, \pm1$ is the hadron's spin projection on $\boldsymbol{S}$.[2] The formal definition of TMDs also contains a gauge link connecting the quark fields, which arises from the gluons, to ensure the gauge invariance [59,60]. Here, we approximate it to be unity for the study of T-even TMDs as other model studies [8,9,28,61].

At leading twist, there are nine time-reversal even TMDs entering the parametrization of $\Theta^{(\Lambda)s}_{\beta\alpha}(x,\boldsymbol{k}_T)$, i.e., [25,27]

$$\frac{1}{2}\mathrm{Tr}_D[\gamma^+\Theta^{(\Lambda)s}(x,\boldsymbol{k}_T)] = f_1(x,\boldsymbol{k}_T^2) + S_{LL}f_{1LL}(x,\boldsymbol{k}_T^2) + \frac{\boldsymbol{S}_{LT}\cdot\boldsymbol{k}_T}{m_V}f_{1LT}(x,\boldsymbol{k}_T^2) + \frac{\boldsymbol{k}_T\cdot\boldsymbol{S}_{TT}\cdot\boldsymbol{k}_T}{m_V^2}f_{1TT}(x,\boldsymbol{k}_T^2), \tag{10}$$

$$\frac{1}{2}\mathrm{Tr}_D[\gamma^+\gamma_5\Theta^{(\Lambda)s}(x,\boldsymbol{k}_T)] = \Lambda\left[S_L g_{1L}(x,\boldsymbol{k}_T^2) + \frac{\boldsymbol{k}_T\cdot\boldsymbol{S}_T}{m_V}g_{1T}(x,\boldsymbol{k}_T^2)\right], \tag{11}$$

$$\frac{1}{2}\mathrm{Tr}_D[-i\sigma^{+i}\gamma_5\Theta^{(\Lambda)s}(x,\boldsymbol{k}_T)] = \Lambda\left[S_T^i h_1(x,\boldsymbol{k}_T^2) + S_L\frac{k_T^i}{m_V}h_{1L}^\perp(x,\boldsymbol{k}_T^2) + \frac{1}{2m_V^2}(2k_T^i\boldsymbol{k}_T\cdot\boldsymbol{S}_T - S_T^i\boldsymbol{k}_T^2)h_{1T}^\perp(x,\boldsymbol{k}_T^2)\right], \tag{12}$$

with

[2]Note that the Λ in Sec. II is defined in the helicity basis, i.e., setting $\boldsymbol{S} = (0,0,1)$.

$$S_{LL} = (3\Lambda^2 - 2)\left(\frac{1}{6} - \frac{1}{2}S_L^2\right), \tag{13}$$

$$S_{LT}^i = (3\Lambda^2 - 2)S_L S_T^i, \tag{14}$$

$$S_{TT}^{ij} = (3\Lambda^2 - 2)\left(S_T^i S_T^j - \frac{1}{2}S_T^2\delta^{ij}\right), \tag{15}$$

The functions f, g, and h denote the quark polarization for being unpolarized, longitudinally polarized and transversely polarized respectively. The lower index 1 denotes leading twist, and the T and L refers to the hadron polarization. There are three tensor polarized TMDs f_{1LL}, f_{1LT} and f_{1TT} that are specific to spin-one hadron.

The overlap representation of vector meson TMDs in terms of LF-LFWFs have been given by authors in [28], with more details in [26,27]. Introducing the quantity

$$A_{\lambda_q'\Lambda',\lambda_q\Lambda}(x,\boldsymbol{k}_T) = \frac{1}{2(2\pi)^3}\sum_{\lambda_{\bar{q}}}\Phi^{\Lambda'*}_{\lambda_q',\lambda_{\bar{q}}}(x,\boldsymbol{k}_T)\Phi^{\Lambda}_{\lambda_q,\lambda_{\bar{q}}}(x,\boldsymbol{k}_T), \tag{16}$$

the vector meson TMDs overlap representation reads [28]

$$f_1(x,\boldsymbol{k}_T^2) = \frac{1}{3}(A_{+0,+0} + A_{-0,-0} + A_{++,++} + A_{-+,-+} + A_{+-,+-} + A_{--,--}), \tag{17}$$

$$g_{1L}(x,\boldsymbol{k}_T^2) = \frac{1}{2}(A_{++,++} - A_{-+,-+} - A_{+-,+-} + A_{--,--}), \tag{18}$$

$$g_{1T}(x,\boldsymbol{k}_T^2) = \frac{m_V}{2\sqrt{2}\boldsymbol{k}_T^2}(k_T^{(+)}(A_{++,+0} - A_{-+,-0} + A_{+0,+-} - A_{-0,--}) + k_T^{(-)}(A_{+0,++} - A_{-0,-+} + A_{+-,+0} - A_{--,-0})), \tag{19}$$

$$h_1(x,\boldsymbol{k}_T^2) = \frac{1}{2\sqrt{2}}(A_{++,-0} + A_{-0,++} + A_{+0,--} + A_{--,+0}), \tag{20}$$

$$h_{1L}^{\perp}(x,\boldsymbol{k}_T^2) = \frac{m_V}{2\boldsymbol{k}_T^2}(k_T^{(+)}(A_{-+,++} - A_{--,+-}) + k_T^{(-)}(A_{++,-+} - A_{+-,--})), \tag{21}$$

$$h_{1T}^{\perp}(x,\boldsymbol{k}_T^2) = \frac{m_V^2}{\sqrt{2}\boldsymbol{k}_T^4}((k_T^{(+)})^2(A_{-+,+0} + A_{-0,+-}) + (k_T^{(-)})^2(A_{+0,-+} + A_{+-,-0})), \tag{22}$$

$$f_{1LL}(x,\boldsymbol{k}_T^2) = A_{+0,+0} + A_{-0,-0} - \frac{1}{2}(A_{++,++} + A_{-+,-+} + A_{+-,+-} + A_{--,--}), \tag{23}$$

$$f_{1LT}(x,\boldsymbol{k}_T^2) = \frac{m_V}{2\sqrt{2}\boldsymbol{k}_T^2}(k_T^{(+)}(A_{++,+0} + A_{-+,-0} - A_{+0,+-} - A_{-0,--}) + k_T^{(-)}(A_{+0,++} + A_{-0,-+} - A_{+-,+0} - A_{--,-0})), \tag{24}$$

$$f_{1TT}(x,\boldsymbol{k}_T^2) = \frac{m_V^2}{2\sqrt{2}\boldsymbol{k}_T^2}((k_T^{(+)})^2(A_{++,+-} + A_{-+,--}) + (k_T^{(-)})^2(A_{+-,++} + A_{--,-+})). \tag{25}$$

To comply with the leading Fock-state truncation in Eqs. (17)–(25), we rescale our BSE-based LF-LFWFs so that they normalize to unity, for both $\Lambda = 0$ and $\Lambda = \pm 1$ vector mesons respectively i.e.,

$$1 = \sum_{\lambda,\lambda'}\int_0^1 dx \int \frac{d\boldsymbol{k}_T^2}{2(2\pi)^3}|\Phi^{\Lambda,(\mathrm{re})}_{\lambda,\lambda'}(x,\boldsymbol{k}_T)|^2. \tag{26}$$

The rescaled LF-LFWFs $\Phi^{\Lambda=0,(\mathrm{re})}_{\lambda,\lambda'} = N_1\Phi^{\Lambda=0}_{\lambda,\lambda'}$ and $\Phi^{\Lambda=\pm1,(\mathrm{re})}_{\lambda,\lambda'} = N_2\Phi^{\Lambda=\pm1}_{\lambda,\lambda'}$. The (N_1, N_2) are (1.49,1.72), (1.07,1.09), and approximately (1.0,1.0) for ρ, J/ψ and Υ respectively. The decreasing N_1 and N_2 indicate the reduction of potential higher Fock-state contributions from light to heavy mesons. In this way, the vector mesons are approximated as a pair of bounded effective quark and antiquark at certain hadronic scale on the light front. In heavy meson this approximation is good, as the higher Fock-states are suppressed. For light meson as ρ, it is less good yet we explore its predictions and compare with other model studies.

Most TMDs are stable in profile under the rescaling procedure, which can be seen from their overlap representation. For instance, in Eqs. (18), (21), (25), the g_{1L}, $h_{1L}^{\perp}$ and f_{1TT} only contain overlapping LF-LFWFs of $\Lambda = \pm 1$,

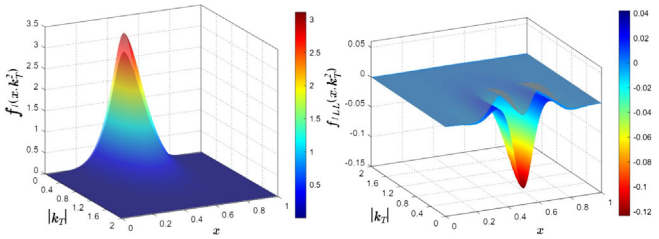

FIG. 1. A demonstration of the J/ψ's $f_1(x,\boldsymbol{k}_T^2)$ (left column) and $f_{1LL}(x,\boldsymbol{k}_T^2)$ (right column) calculated using rescaled (colored surface) and unrescaled (gray surface) LF-LFWFs.

so these TMDs change by an overall factor N_2^2 after rescaling. Similarly, the g_{1T}, h_1, $h_{1T}^{\perp}$, and f_{1LT}, take overlaps between LF-LFWFs of $\Lambda = 0$ and $\Lambda = \pm 1$, so they get an overall factor $N_1 N_2$. The f_1 and f_{1LL}, however, do not have an overall factor. The f_1 is the average of the unpolarized TMDs of $\Lambda = 0$ and $\Lambda = \pm 1$ meson. Since N_1 and N_2 do not differ much (15% at most in ρ), the profile of f_1 does not change much either. The f_{1LL}, however, is the difference between the unpolarized TMDs of $\Lambda = 0$ and $\Lambda = \pm 1$. The cancellation end up being rather sensitive to N_1/N_2, and f_{1LL} can change dramatically under the rescaling procedure. This is demonstrated in Fig. 1 for the case of J/ψ. This indicates that f_{1LL} demands careful treatment on higher Fock-state effects, and the rescaling procedure could bring large uncertainties in this respect. We therefore leave $f_{1LL}(x,\boldsymbol{k}_T^2)$ out in this work (for most of the study) and focus on the rest of the TMDs.

Finally, we remark that in real QCD, the rigorous definition of TMDs contains two scales, i.e., the renormalization scale μ_0 associated with UV divergence, and the so-called Collins-Soper scale ζ_0 associated with rapidity divergence [60,62–65]. In model and phenomenological studies [10,16,17,61], the ζ_0 is usually set to μ_0^2. On the other hand, the leading Fock-state approximation implicitly sets the scale of our TMDs. In this work, we follow earlier study on pseudoscalar mesons [54] and approximate the scale of our TMDs to be $\mu_0 \approx 2m_f$ [66]. The m_f is defined as the Eucledian constituent quark mass which satisfies $M_f(q^2 = m_f^2) = m_f^2$ where $M_f(q^2)$ is the quark mass function of flavor f. For heavy mesons, we obtain $\mu_0 \approx 2.6$ GeV for J/ψ and $\mu_0 \approx 8.6$ GeV for Υ TMDs. For ρ, we obtain $\mu_0 \approx 0.6$ GeV. As will be addressed in Sec. IV, by evolving and comparing the collinear PDF with lattice prediction, we finally determine the renormalization scale of our ρ TMDs to be $\mu_0 \approx 0.67$ GeV.

IV. RESULTS

A. TMDs of J/ψ and Υ

We show in Fig. 2 the TMDs $f_1(x,\boldsymbol{k}_T^2)$, $g_{1L}(x,\boldsymbol{k}_T^2)$, and $h_1(x,\boldsymbol{k}_T^2)$ of J/ψ (left column) and Υ (right column), which have one-dimensional correspondences, e.g., the collinear

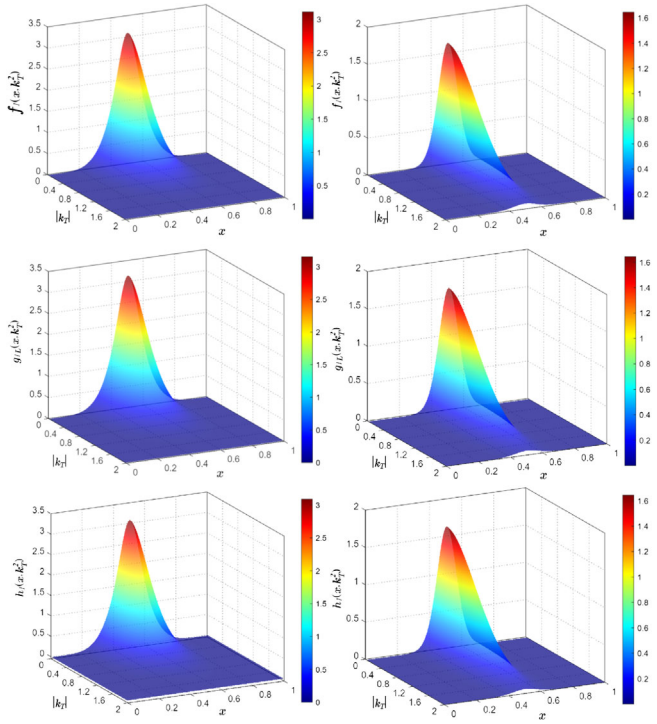

FIG. 2. 3D plot of the $f_1(x,\boldsymbol{k}_T^2)$ (top row), $g_{1L}(x,\boldsymbol{k}_T^2)$ (middle row), and $h_1(x,\boldsymbol{k}_T^2)$ (bottom row) for J/ψ (left column) and Υ (right column).

PDF $f_1(x)$, $g_{1L}(x)$, and $h_1(x)$ respectively.[3] They describe the momentum distribution of unpolarized, longitudinally polarized and transversely polarized quarks in mesons with the same polarization. These TMDs are similar in profile and magnitude within the same meson. They are mostly centered at $x = 1/2$ and low $\boldsymbol{k}_T^2$ and decrease monotonically, indicating the heavy quark and the antiquark tend to have low relative momentum. Meanwhile, f_1 is symmetric with respect to $x = 1/2$, while the g_{1L} and h_1 are slightly asymmetric. The asymmetry originates from the p- and d-wave LF-LFWFs; in Eqs. (17), (18), and (20) the overlapping LF-LFWFs are diagonal in l_z for f, g_{1L}, and h_1, so the p- and d-wave contributions to these TMDs can be separated from the s-wave contribution. Given that the p- and d-wave LF-LFWFs are suppressed in heavy mesons, the asymmetry is thus slight. From J/ψ to Υ, the TMDs get narrower in x but broader in $\boldsymbol{k}_T^2$. Therefore, the quark and antiquark in a heavier meson tend to carry larger transverse momentum but smaller relative longitudinal momentum.

We then show the worm-gear TMDs g_{1T}, $h_{1L}^{\perp}$ and the pretzelosity TMD $h_{1T}^{\perp}$ in Fig. 3. The g_{1T} describes the momentum distribution of the longitudinally-polarized quark in transversely-polarized meson, while $h_{1L}^{\perp}$ and

[3]We use the same notation for TMD and collinear PDF for convenience. They can be easily distinguished based on the context.

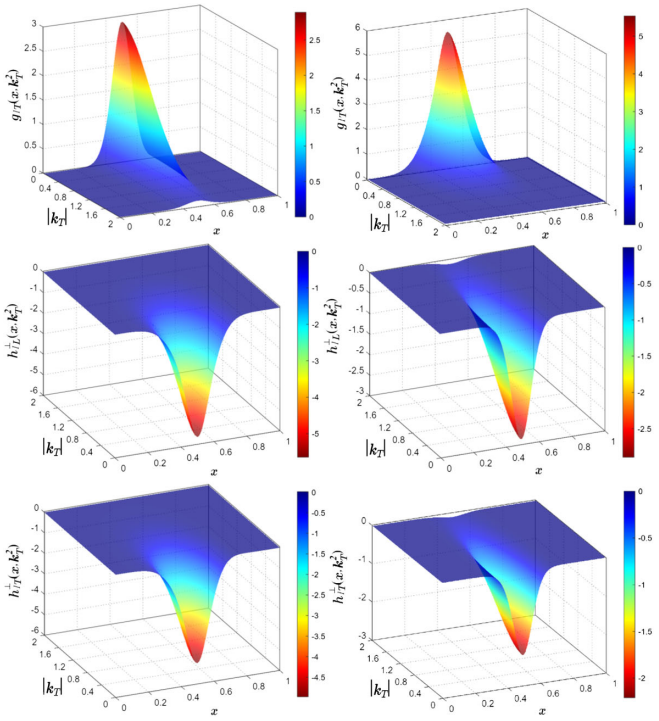

FIG. 3. 3D plot of the $g_{1T}(x,\boldsymbol{k}_T^2)$ (top row), $h_{1L}^{\perp}(x,\boldsymbol{k}_T^2)$ (middle row), and $h_{1T}^{\perp}(x,\boldsymbol{k}_T^2)$ (bottom row) for J/ψ (left column) and Υ (right column).

$h_{1T}^{\perp}$ are for the transversely-polarized quark in longitudinally and transversely-polarized (perpendicular to quark polarization) mesons, respectively. These TMDs are similar in magnitude, with $h_{1L}^{\perp}$ and $h_{1T}^{\perp}$ being negative. They are generally not symmetric in $x \to 1-x$. From Eqs. (19) and (21) one observes that the g_{1T} and $h_{1L}^{\perp}$ only include overlaps between LF-LFWFs that differ by one unit in OAM, i.e., $|\Delta l_z| = 1$, while for $h_{1T}^{\perp}$ the overlapping LF-LFWFs differ by $|\Delta l_z| = 2$. Since our LF-LFWFs are nonvanishing for all possible l_z components, the TMDs are nonvanishing as well. We remark that although the worm-gear and pretzelosity TMDs in Fig. 3 appear larger in magnitude than f_1, g_{1L}, and h_1, their contributions to the correlation function are actually suppressed by factors proportional to $|\boldsymbol{k}_T|/m_V$ or $(|\boldsymbol{k}_T|/m_V)^2$ from Eqs. (11) and (12), given that the TMDs of J/ψ and Υ have typical support in $|\boldsymbol{k}_T| < 1$ GeV in Fig. 3.

Finally, the tensor polarized TMDs f_{1LT} and f_{1TT} are shown in Fig. 4. They are significantly smaller in magnitude as compared to other TMDs. We find f_{1LT} is antisymmetric with respect to $x = 1/2$ while f_{1TT} is symmetric. Based on Eqs. (24) and (25), the f_{1LT} is the overlap between LF-LFWFs of $\Lambda = 0$ and $\Lambda = \pm 1$ with one unit of OAM ($\Delta l_z| = 1$) transfer while f_{1TT} is the overlap between $\Lambda = +1$ and $\Lambda = -1$ LF-LFWFs with two units of OAM transfer, i.e., $|\Delta l_z| = 2$. The f_{1LT} and f_{1TT} are quite different in profile between J/ψ and Υ, which was not observed for previously shown TMDs. This indicates

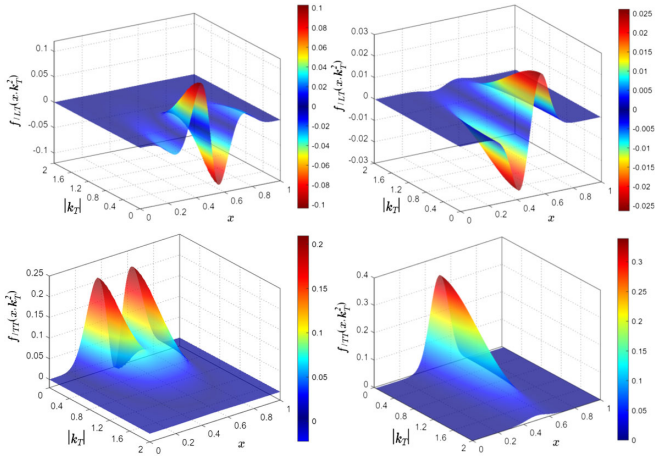

FIG. 4. 3D plot of the $f_{1LT}(x,\boldsymbol{k}_T^2)$ (top row) and $f_{1TT}(x,\boldsymbol{k}_T^2)$ (bottom row) for J/ψ (left column) and Υ (right column).

that they are sensitive to the current mass of valence quarks in the vector mesons.

B. TMDs of ρ

We show the calculated ρ TMDs in Fig. 5. As compared to the TMDs of heavy vector mesons, they are significantly broader in x and narrower in $\boldsymbol{k}_T^2$, following the trend from Υ to J/ψ. We recall that such an effect is also observed in the TMDs of light and heavy pseudoscalar mesons [54]. On the other hand, the ρ meson is a highly-relativistic system, so the p- and d-wave LF-LFWFs are more pronounced. They bring prominent effect, as the g_{1L}, h_1, g_{1T}, $h_{1L}^{\perp}$, and $h_{1T}^{\perp}$ become more asymmetric.[4] Meanwhile, the f_{1LT} and f_{1TT} are strongly enhanced as compared to those in J/ψ and Υ. Note that f_{1LT} and f_{1TT} undergo a flip in sign from ρ to Υ.

It is interesting to compare our ρ TMDs with those from the NJL model [27], the light front holographic model and the light front quark model [28]. In particular, it is found that the light front holographic model agrees well with NJL model on the profile of all the ρ TMDs, i.e., the TMDs share exactly same behavior such as being vanishing or nonvanishing, positive, or negative, as well as the way they are skewed [28]. Here, we want to point out that, such nice agreement could be due to the fact that the two models actually have LF-LFWFs with the same nonvanishing spin configurations. To see that, we first recapitulate the light front holographic LFWFs of ρ, which read [28,67]

$$\Phi_{\lambda,\lambda'}^{\Lambda=0}(x,\boldsymbol{k}_T) = N_L \delta_{\lambda,-\lambda'}(m_\rho^2 x(1-x) + m_q^2 + \boldsymbol{k}_T^2)\frac{\psi(x,\boldsymbol{k}_T^2)}{x(1-x)}, \tag{27}$$

[4]The g_{1L} and h_1 are asymmetric at $\boldsymbol{k}_T^2 \neq 0$, which would be more obvious by plotting $|\boldsymbol{k}_T| g_{1L}$ and $|\boldsymbol{k}_T| h_1$ instead.

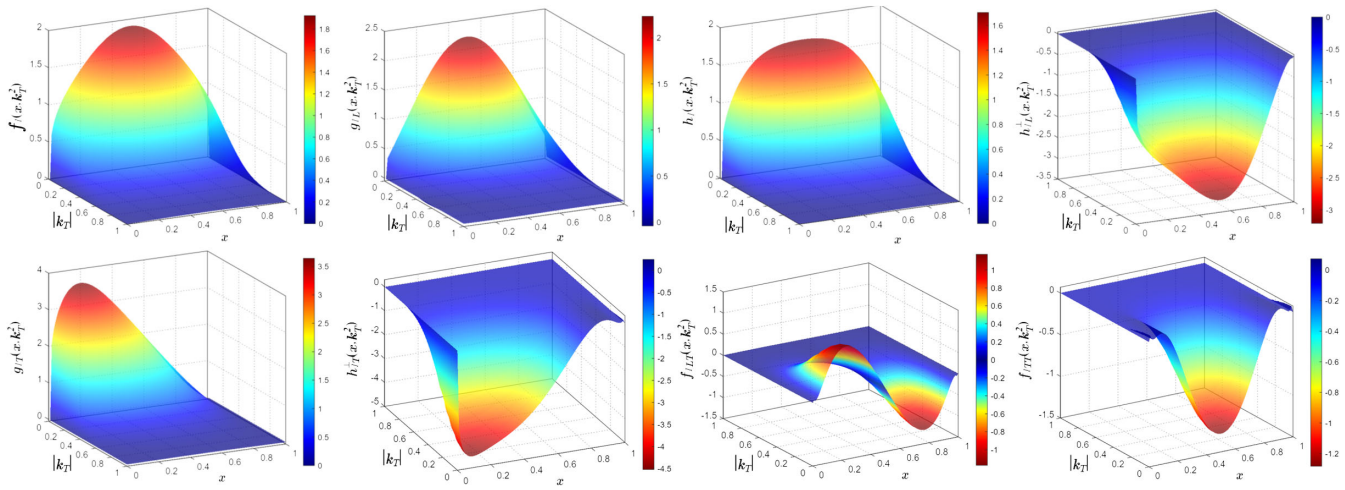

FIG. 5. The ρ TMDs from the full BSE-based LF-LFWFs.

$$\Phi^{\Lambda=\pm1}_{\lambda,\lambda'}(x,\boldsymbol{k}_T) = N_T[|\boldsymbol{k}_T|e^{\pm i\theta_{k_T}}(\pm x\delta_{\lambda\pm,\lambda'\mp} \mp (1-x)\delta_{\lambda\mp,\lambda'\pm}) + m_q\delta_{\lambda\pm,\lambda'\pm}]\frac{\psi(x,\boldsymbol{k}_T^2)}{x(1-x)}. \tag{28}$$

Here, $\delta_{ab,cd} = \delta_{a,b}\delta_{c,d}$, with $\delta_{a,b}$ the Kronecker delta. The spin configurations are generated by the bare vertex γ_μ with

$$\frac{\bar{u}_\lambda(k^+,\boldsymbol{k}_T)}{\sqrt{x}}\epsilon_\Lambda\cdot\gamma\frac{v_{\lambda'}(k'^+,\boldsymbol{k}'_T)}{\sqrt{1-x}}. \tag{29}$$

The k and k' denotes the four-momenta of the quark and antiquark, respectively. They satisfy $k^+ = xP^+$, $k'^+ = (1-x)P^+$ and $\boldsymbol{k}_T = -\boldsymbol{k}_T$, where P is the meson four-momentum. Comparing with Eqs. (3) and (4), one finds that $\Phi^{\Lambda=0}_{\pm,\pm}$ and $\Phi^{\Lambda=\pm1}_{\mp,\mp}$ vanish in Eqs. (27) and (28). Note that $\Phi^{\Lambda=0}_{\pm,\pm}$ and $\Phi^{\Lambda=\pm1}_{\mp,\mp}$ correspond to $|l_z|=1$ and $|l_z|=2$ respectively, so we will denote them as $\Phi^{\Lambda=0}_{|l_z|=1}$ and $\Phi^{\Lambda=\pm1}_{|l_z|=2}$ in the following. On the other hand, the NJL model calculation takes the covariant formalism rather than the light front overlap formalism. We can follow Eq. (29), or equivalently Eq. (2), and project out the LF-LFWFs from ρ's Bethe-Salpeter amplitude in the NJL model. We recall that the Dirac structure of ρ's BS amplitude contains only the γ_μ term, see Eq. (47) in [27], so it generates exactly the same spin configurations as light front holographic model does.

To make an analogous comparison with the light front holographic model, we set $\Phi^{\Lambda=0}_{|l_z|=1}$ and $\Phi^{\Lambda=\pm1}_{|l_z|=2}$ of the BSE-based LF-LFWFs to zero, and recalculate all the TMDs. While some TMDs do not change much, significant deviations are found in others which we have picked out and plotted in Fig. 6. One can see by comparing the second row of Fig. 5 to Fig. 6, the g_{1T} changes from asymmetric in x to symmetric, and the $h^\perp_{1T}$ changes from nonvanishing to vanishing. Moreover, the f_{1LT} and f_{1TT} both undergo a sign flip. The LF-LFWFs with higher OAM thus have sizable effect in determining these TMDs. It is worth noting that the TMDs in Fig. 6 plus the first row of Fig. 5 agree very well with the light front holographic model or the NJL model regarding their profiles. Again, we remark that although the $g_{1T}, h^\perp_{1L}$, and $h^\perp_{1T}$ are larger in magnitude as compared to other TMDs, their contribution to the correlation function is suppressed by powers of $|\boldsymbol{k}_T|/m_\rho$, with $|\boldsymbol{k}_T|$ typically around 0.3 GeV. Similar observation had been made in [27].

Finally, we remark that the light front quark model incorporates nonvanishing $\Phi^{\Lambda=0}_{|l_z|=1}$ and $\Phi^{\Lambda=\pm1}_{|l_z|=2}$ [68,69], and yields g_{1T} and $h^\perp_{1T}$ which are similar to ours in Fig. 5 [28]. However, the tensor-polarized TMDs f_{1LT} and f_{1TT} vanish in the light front quark model, which is different from our

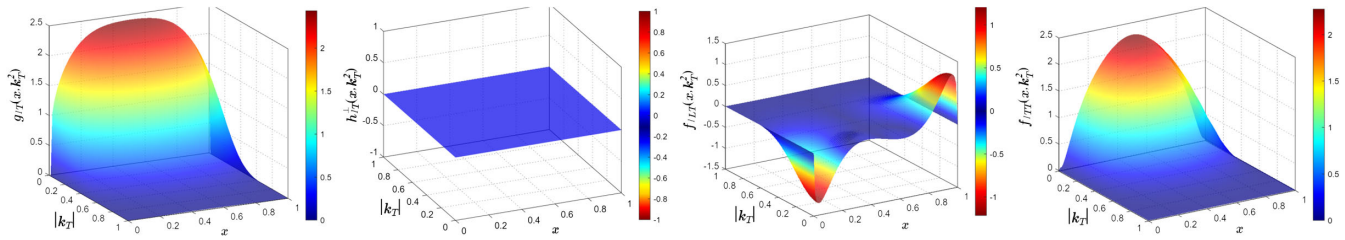

FIG. 6. The ρ TMDs obtained by setting $\phi^{\Lambda=0}_{|l_z|=1} = \phi^{\Lambda=1}_{|l_z|=2} = 0$ in the full BSE-based LF-LFWFs.

TABLE II. The $\boldsymbol{k}_T$-moment of TMDs defined in Eq. (30). Lines in the blank indicate the corresponding TMDs are vanishing. All units are given in GeV. The first three columns are taken from [27,28].

	$\langle \boldsymbol{k}_T\rangle^{\rho}_{\mathrm{NJL}}$	$\langle \boldsymbol{k}_T\rangle^{\rho}_{\mathrm{LFHM}}$	$\langle \boldsymbol{k}_T\rangle^{\rho}_{\mathrm{LFQM}}$	$\langle \boldsymbol{k}_T\rangle^{\rho}_{\mathrm{BSE}}$	$\langle \boldsymbol{k}_T\rangle^{J/\psi}_{\mathrm{BSE}}$	$\langle \boldsymbol{k}_T\rangle^{\Upsilon}_{\mathrm{BSE}}$
f_1	0.32	0.238	0.328	0.399	0.623	1.020
g_{1L}	0.08	0.204	0.269	0.318	0.589	1.003
g_{1T}	0.34	0.229	0.269	0.358	0.615	1.020
h_1	0.34	0.229	0.307	0.367	0.608	1.012
$h_{1L}^{\perp}$	0.33	0.204	0.269	0.368	0.608	1.017
$h_{1T}^{\perp}$	…	…	0.237	0.365	0.602	1.017
f_{1TT}	0.32	0.211	…	0.338	0.764	1.063

result. So at this stage, new possibilities regarding the profile of f_{1LT} and f_{1TT} are presented in Fig. 5.

C. Integrated TMDs

To quantify the transverse momentum dependence in TMDs and compare with other model studies, we follow [27,28] and calculate the mean transverse momentum of certain TMDs, defined through

$$\langle \boldsymbol{k}_T\rangle = \frac{\int dx\, d^2\boldsymbol{k}_T |\boldsymbol{k}_T| \mathcal{F}(x,\boldsymbol{k}_T^2)}{\int dx\, d^2\boldsymbol{k}_T \mathcal{F}(x,\boldsymbol{k}_T^2)}, \tag{30}$$

where the $\mathcal{F}$ stands for various TMDs. These $\langle \boldsymbol{k}_T\rangle$'s therefore characterize the "broadness" of the $\boldsymbol{k}_T-$ distribution of the TMDs. We note that this definition is highly empirical and works only for model study purposes, as in real QCD the momentum integration in both the numerator and denominator could suffer from divergences [59,70]. In Table. II, we list the $\langle \boldsymbol{k}_T\rangle$ of concerned TMDs, and compare with other model studies. Our result is listed in the last three columns. We notice that our results on ρ are generally larger than other model predictions, but are close to the NJL model for most TMDs. We note that these values are obtained at low-hadronic scale. As the renormalization scale increases, the $|\boldsymbol{k}_T|-$dependence would evolve. In addition to the unpolarized TMD, the polarized TMDs evolution has been investigated [71–73]. For instance, it was found in [71] that the polarized TMDs, i.e., g_{1L} and h_1, evolve in the same way as unpolarized TMD f_1. So the polarization only affect TMD evolution through the collinear factorization of the TMDs in terms of collinear PDFs in the small $|\boldsymbol{b}_T|$ region.[5] The final finding was that all the TMDs get broader in $|\boldsymbol{k}_T|$ after evolving to a higher scale. We therefore anticipate the vector meson TMDs to get broader in $|\boldsymbol{k}_T|$ as the scale increases as well.

In our model study, the collinear PDFs of vector mesons can be obtained by integrating over the $\boldsymbol{k}_T$ in TMDs, i.e.,

$$\mathcal{F}(x) = \int d\boldsymbol{k}_T^2 \mathcal{F}(x,\boldsymbol{k}_T^2), \tag{31}$$

with $\mathcal{F} = f_1, g_{1L}, h_1$ and f_{1LL}. The $f_1(x)$ has the probabilistic interpretation of finding an unpolarized quark in an unpolarized meson. The helicity PDF g_{1L} is the number density of quarks with helicity 1 over quarks with helicity -1 in a meson with helicity 1, and the transversity PDF h_1 is the analog when both quarks and mesons are transversely polarized along the same axis. The f_{1LL} characterizes the difference of unpolarized quark distribution between $\Lambda = 0$ and $\Lambda = \pm 1$ states. We stress again that Eq. (31) is restricted to a model study, but does not hold true in QCD [59,70]. Meanwhile the parton-density interpretation is only valid for leading-order QCD.

We plot the PDFs f_1, g_{1L}, and h_1 of ρ, J/ψ, and Υ in Fig. 7. The PDFs of heavy mesons are generally narrow in x and centered around $x = 1/2$. Meanwhile, PDFs of the same heavy meson are quite close to each other. Looking into the quark spin sum $\langle x^0\rangle_{g_{1L}} = \int dx g_{1L}(x)$ and tensor charge $\langle x^0\rangle_{h_1} = \int dx h_1(x)$, we find $\langle x^0\rangle^{J/\psi}_{g_{1L}} = 0.92$, $\langle x^0\rangle^{J/\psi}_{h_1} = 0.96$ and $\langle x^0\rangle^{\Upsilon}_{g_{1L}} = 0.98$, $\langle x^0\rangle^{\Upsilon}_{h} = 0.99$. They are less than unity due to nonzero OAM of quarks, and closer to unity in Υ than in J/ψ, as the relativistic effect reduces. We note that these results are in qualitative agreement with those by the BLFQ approach and light front models [66,74,75]. On the other hand, the PDFs of ρ are much broader and the deviation between the PDFs are more significant. This indicates the quark and antiquark in a highly-relativistic system as ρ are no longer constrained to carry small relative longitudinal momentum as in heavy mesons. Moreover, nonzero OAM configurations become significant as we find $\langle x^0\rangle^{\rho}_{g_{1L}} = 0.67$ and $\langle x^0\rangle^{\rho}_{h_1} = 0.79$.

While the ρ PDFs are unavailable by experiment, lattice QCD has made predictions on their moments [76,77]. In [76], the first three moments of ρ's valence (nonsinglet)

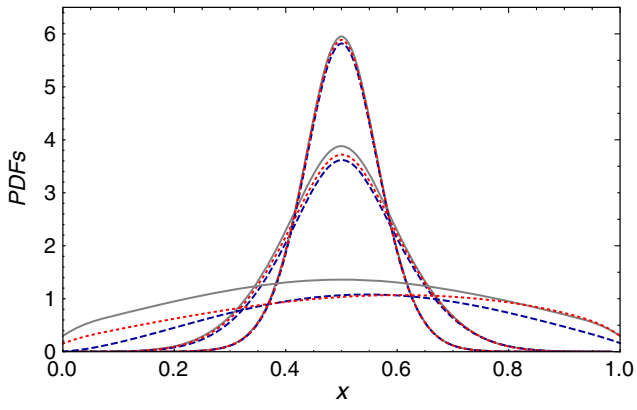

FIG. 7. The $f_1(x)$ (gray solid), $g_{1L}(x)$ (red dotted) and $h_1(x)$ (blue dashed) of vector mesons at hadron scale. At $x = 0.5$, from top to bottom, the three sets of curves correspond to Υ, J/ψ, and ρ respectively.

[5]The TMD evolution is conveniently performed in the $\boldsymbol{b}_T$ space, which is the Fourier conjugate of $\boldsymbol{k}_T$.

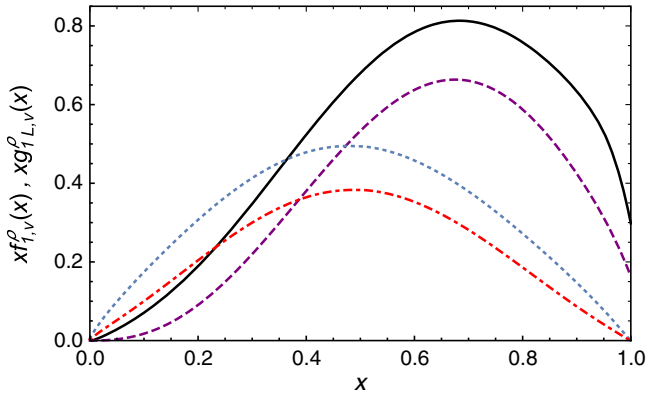

FIG. 8. The $xf^{\rho}_{1,v}(x)$ at hadronic scale (black solid) and evolved scale of 2.4 GeV (blue dotted), and $xg^{\rho}_{1L,v}(x)$ at hadronic scale (purple dashed) and evolved scale of 2.4 GeV (red dot-dashed).

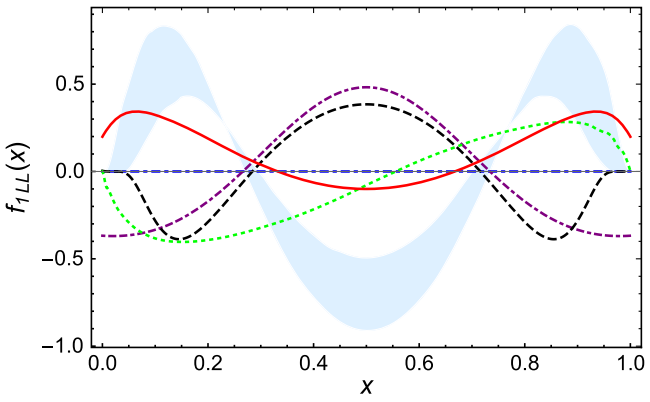

FIG. 9. The tensor polarized PDF $f_{1LL}(x)$ of ρ from light front constituent quark model [81] (green dotted), LF quark model [28] (blue dot-dashed), NJL model [27](purple dot-dash-dashed), light front holographic model [28] (black dashed), [82] (light blue band) and unrescaled BSE-based LF-LFWFs (red solid). Note that only the large-x part of red solid curve is meaningful.

unpolarized distribution $a_n = \langle x^{n-1} \rangle_{f_{1,v}}$ and helicity distribution $r_n = \langle x^{n-1} \rangle_{g_{1L,v}}$ at a renormalization scale of $\mu \approx 2.4$ GeV are given

$$a_2 = 0.334(21), \qquad a_3 = 0.174(47), \qquad a_4 = 0.066(39), \tag{32}$$

$$r_1 = 0.57(32), \qquad r_2 = 0.212(17), \qquad r_3 = 0.077(34). \tag{33}$$

Note in [76], there are two sets of r_n values extracted from two different operators which should equal in the continuum limit. Here, we take their intersection. To compare with the lattice prediction directly, we evolve our PDFs to the scale of $\mu_2 = 2.4$ GeV using the NLO-DGLAP evolution with the help from the QCDNUM package [78]. The strong coupling constant is set to the optimal value in NLO global PDF analysis $\alpha_s(1\ \text{GeV}) = 0.491$ [79] and the variable flavor number scheme is taken. However, the initial scale of our ρ PDFs model is unknown. Here, we choose it to be $\mu_0 = 670$ MeV.[6] In this case, the valence ρ PDFs at scales μ_0 and μ_2 are shown in Fig. 8, with the later yield

$$a_2 = 0.316, \qquad a_3 = 0.155, \qquad a_4 = 0.091, \tag{34}$$

$$r_1 = 0.66, \qquad r_2 = 0.227, \qquad r_3 = 0.111. \tag{35}$$

at the scale of 2.4 GeV. They agree with lattice predictions in Eqs. (32) and (33) within uncertainties.

Ref. [76] also predicted the moments of valence tensor polarized PDF $f_{1LL,v}(x)$. However, due to the instability of $f_{1LL}(x)$ under the rescaling procedure, we refrain from making prediction on its moments, as the latter relies on $f_{1LL}(x)$'s global behavior at all x. On the other hand, model studies have given diverse predictions on $f_{1LL}(x)$ so far, as displayed in Fig. 9. In this respect, our LF-LFWFs can shed some light on the $f_{1LL}(x)$'s behavior at relatively large x, e.g., $x \gtrsim 0.8$, since the large x behavior of PDFs, i.e., $x \to 1$, is dominated by LF-LFWFs [80]. So we plot $f_{1LL}(x)$ calculated with our original (unrescaled) ρ LF-LFWFs as the solid curve in Fig. 9. We emphasize that only the large x region of the solid curve is meaningful in such scheme. We find our $f_{1LL}(x)$ is positive at large x, similar to results of [81,82]. Meanwhile, the light front quark model gives a vanishing result [28], and the NJL model and the LF holographic model give a negative result [27,28]. Such a discrepancy deserves careful investigation in the future. For instance, a potential solution could be to carry out a fully covariant calculation of ρ's f_{1LL} in analogy to the pion PDF calculation [83], so that higher Fock-state effects can be counted in.

V. SUMMARY

We extend the study of ρ and J/ψ LF-LFWFs in [38] to extract the LF-LFWFs of Υ from its BS wave functions. The leading Fock-state approximation is then enforced by rescaling the LF-LFWFs, and the TMDs of ρ, J/ψ, and Υ are studied using the light front overlap representation. Among all the nine TMDs, the f_{1LL} is unstable under the rescaling procedure, indicating its sensitivity to Fock-state truncation, thus left out in this study.

For J/ψ and Υ, we find the unpolarized, longitudinally-polarized, and transversely-polarized TMDs are all sizable in magnitude, while the tensor-polarized TMDs f_{1LT} and f_{1TT} are suppressed. The tensor-polarized TMDs change

[6]The corresponding expansion parameter of perturbative NLO-DGLAP evolution is $\frac{\alpha_s(\mu_0)}{2\pi} = 0.126$.

significantly from J/ψ to Υ, indicating their sensitivity to the quark mass. All TMDs in heavy mesons appear symmetric with respect to $x = 1/2$ due to the suppressed p- and d-wave LF-LFWFs.

The ρ TMDs are then explored and compared with existing studies by the light front holographic model, the NJL model and the light front quark model [27,28]. The ρ TMDs are generally broad in x and concentrate in low $\boldsymbol{k}_T^2$. We point out both the light front holographic model and the NJL model have $\Phi^{\Lambda=0}_{|l_z|=1} = \Phi^{\Lambda=\pm1}_{|l_z|=2} = 0$, and after enforcing this condition on the BSE-based LF-LFWFs similar TMDs can be obtained. Our final result on ρ TMDs is given in Fig. 5. In this case, the g_{1T} and $h_{1T}^{\perp}$ are found to agree with the light front quark model, while the profiles of f_{1LT} and f_{1TT} are new in literature. We therefore argue that LF-LFWFs with higher OAM can have sizable impact in determining certain polarized TMDs. We also compare the $\boldsymbol{k}_T$ dependence of our ρ TMDs with these models and general agreement is found in Table. II. We stress that the comparison herein is made at a low hadronic scale, i.e., roughly between 500–670 MeV. Evolution to higher scales should broaden these TMDs.

Finally, the collinear PDFs of ρ, J/ψ and Υ are studied. We evolve our ρ valence PDFs, i.e., $f_{1,v}(x)$ and $g_{1L,v}(x)$, to the scale of 2.4 GeV. The first three moments of these PDFs are found to be in agreement with lattice prediction within uncertainties [76]. We also calculate the $f_{1LL}(x)$ using unrescaled BSE-based LF-LFWFs, and find it to be positive at large x. A covariant calculation that counts in the higher Fock-states effects on $f_{1LL}(x)$ is thus called for.

ACKNOWLEDGMENTS

We thank Professor Fan Wang for helpful suggestions. This work is supported by the National Natural Science Foundation of China (Grant No. 11905104) and the Strategic Priority Research Program of Chinese Academy of Sciences (Grant No. XDB34030301).

APPENDIX: LF-LFWFs OF VECTOR MESONS

The LF-LFWFs of ρ and J/ψ mesons from Dyson-Schwinger equations approach have been reported in [38]. Here we supplement with LF-LFWFs of Υ and show all the LF-LFWFs in Figs. 10and 11.

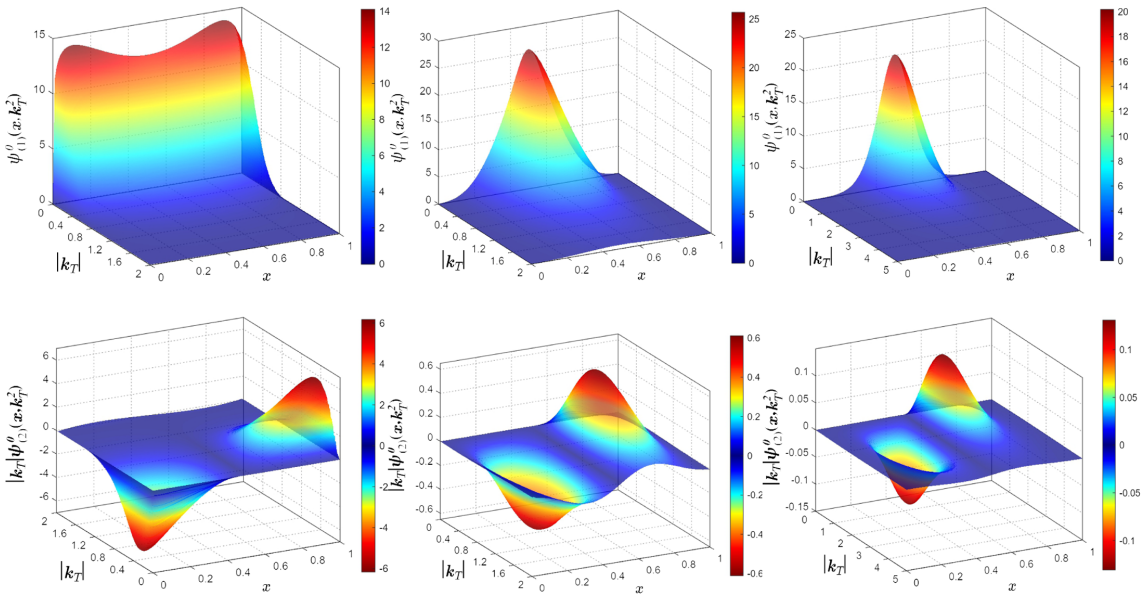

FIG. 10. The LF-LFWFs of ρ (left column), J/ψ (middle column), and Υ (right column) with $\Lambda = 0$. See Eqs. (1), (3), and (4) for definition of the LF-LFWFs.

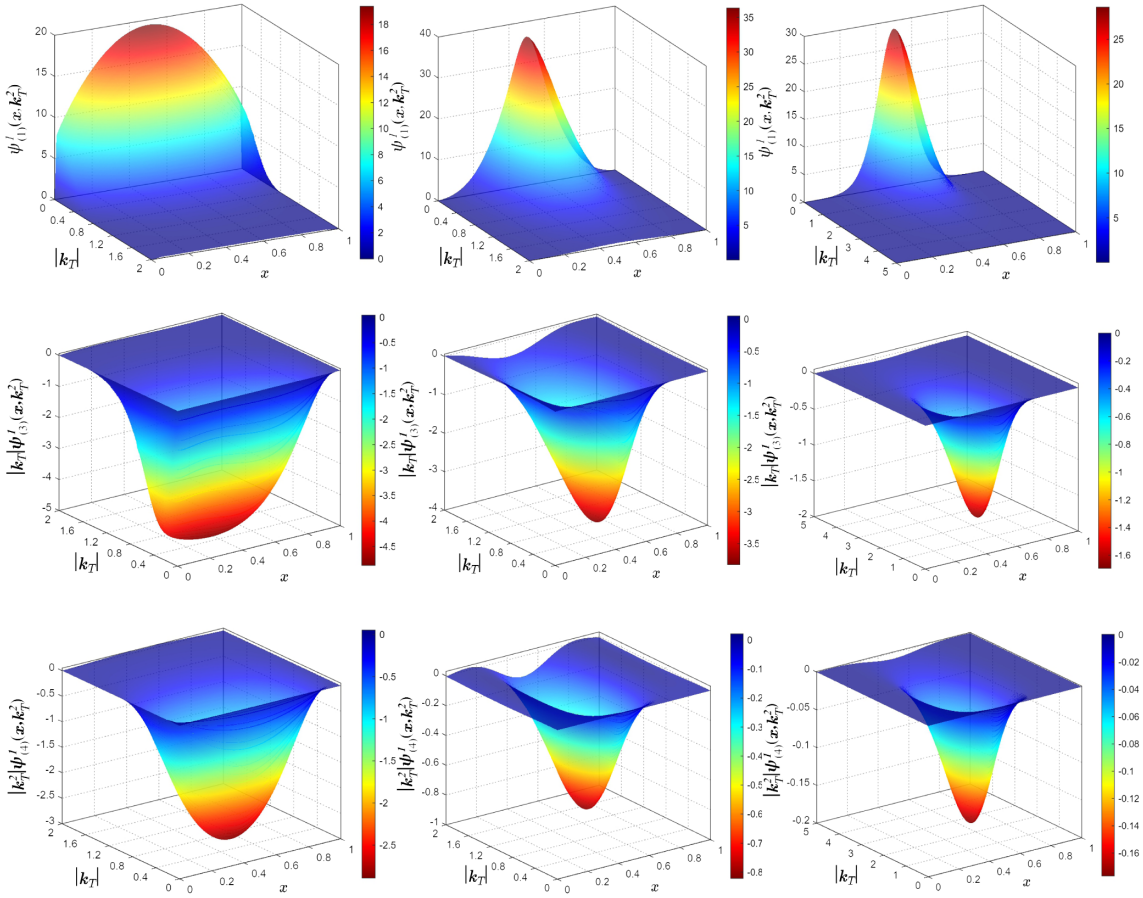

FIG. 11. The LF-LFWFs of ρ (left column), J/ψ (middle column), and Υ (right column) with $\Lambda = \pm 1$. See Eqs. (1), (3), and (4) for definition of the LF-LFWFs.

[1] D. W. Sivers, Phys. Rev. D **41**, 83 (1990).
[2] D. Boer and P. J. Mulders, Phys. Rev. D **57**, 5780 (1998).
[3] V. Barone, A. Drago, and P. G. Ratcliffe, Phys. Rep. **359**, 1 (2002).
[4] R. Angeles-Martinez *et al.*, Acta Phys. Pol. B **46**, 2501 (2015).
[5] B. Pasquini, M. Pincetti, and S. Boffi, Phys. Rev. D **72**, 094029 (2005).
[6] A. Bacchetta, F. Conti, and M. Radici, Phys. Rev. D **78**, 074010 (2008).
[7] B. Pasquini, S. Cazzaniga, and S. Boffi, Phys. Rev. D **78**, 034025 (2008).
[8] B. Pasquini and P. Schweitzer, Phys. Rev. D **90**, 014050 (2014).
[9] S. Noguera and S. Scopetta, J. High Energy Phys. 11 (2015) 102.
[10] C. Shi and I. C. Cloët, Phys. Rev. Lett. **122**, 082301 (2019).
[11] M. Engelhardt, P. Hägler, B. Musch, J. Negele, and A. Schäfer, Phys. Rev. D **93**, 054501 (2016).
[12] M. A. Ebert, I. W. Stewart, and Y. Zhao, J. High Energy Phys. 09 (2019) 037.
[13] Q.-A. Zhang *et al.* (Lattice Parton Collaboration), Phys. Rev. Lett. **125**, 192001 (2020).
[14] Y. Li *et al.*, Phys. Rev. Lett. **128**, 062002 (2022).
[15] A. Bacchetta, M. Diehl, K. Goeke, A. Metz, P. J. Mulders, and M. Schlegel, J. High Energy Phys. 02 (2007) 093.
[16] X. Wang, Z. Lu, and I. Schmidt, J. High Energy Phys. 08 (2017) 137.
[17] A. Bacchetta, F. Delcarro, C. Pisano, M. Radici, and A. Signori, J. High Energy Phys. 06 (2017) 081; 06 (2019) 051 (E).
[18] I. Scimemi and A. Vladimirov, Eur. Phys. J. C **78**, 89 (2018).
[19] A. Vladimirov, J. High Energy Phys. 10 (2019) 090.
[20] M. Bury, A. Prokudin, and A. Vladimirov, Phys. Rev. Lett. **126**, 112002 (2021).
[21] P. Hoodbhoy, R. L. Jaffe, and A. Manohar, Nucl. Phys. **B312**, 571 (1989).

[22] A. V. Efremov and O. V. Teryaev, Sov. J. Nucl. Phys. **36**, 557 (1982), https://inspirehep.net/literature/171155.
[23] F. E. Close and S. Kumano, Phys. Rev. D **42**, 2377 (1990).
[24] A. Airapetian *et al.* (HERMES Collaboration), Phys. Rev. Lett. **95**, 242001 (2005).
[25] A. Bacchetta and P. J. Mulders, Phys. Rev. D **62**, 114004 (2000).
[26] A. Bacchetta and P. J. Mulders, Phys. Lett. B **518**, 85 (2001).
[27] Y. Ninomiya, W. Bentz, and I. C. Cloët, Phys. Rev. C **96**, 045206 (2017).
[28] S. Kaur, C. Mondal, and H. Dahiya, J. High Energy Phys. 01 (2021) 136.
[29] S. Nair, C. Mondal, X. Zhao, A. Mukherjee, and J. P. Vary (BLFQ), Phys. Lett. B **827**, 137005 (2022).
[30] P. Maris, C. D. Roberts, and P. C. Tandy, Phys. Lett. B **420**, 267 (1998).
[31] P. Maris and P. C. Tandy, Phys. Rev. C **60**, 055214 (1999).
[32] A. Bacchetta, M. Boglione, A. Henneman, and P. J. Mulders, Phys. Rev. Lett. **85**, 712 (2000).
[33] G. 't Hooft, Nucl. Phys. **B75**, 461 (1974).
[34] H. H. Liu and D. E. Soper, Phys. Rev. D **48**, 1841 (1993).
[35] M. Burkardt, X.-d. Ji, and F. Yuan, Phys. Lett. B **545**, 345 (2002).
[36] C. Mezrag, H. Moutarde, and J. Rodriguez-Quintero, Few Body Syst. **57**, 729 (2016).
[37] W. de Paula, E. Ydrefors, J. H. Alvarenga Nogueira, T. Frederico, and G. Salmè, Phys. Rev. D **103**, 014002 (2021).
[38] C. Shi, Y.-P. Xie, M. Li, X. Chen, and H.-S. Zong, Phys. Rev. D **104**, L091902 (2021).
[39] C. D. Roberts and A. G. Williams, Prog. Part. Nucl. Phys. **33**, 477 (1994).
[40] P. Maris and C. D. Roberts, Int. J. Mod. Phys. E **12**, 297 (2003).
[41] I. C. Cloet and C. D. Roberts, Prog. Part. Nucl. Phys. **77**, 1 (2014).
[42] G. Eichmann, H. Sanchis-Alepuz, R. Williams, R. Alkofer, and C. S. Fischer, Prog. Part. Nucl. Phys. **91**, 1 (2016).
[43] P.-L. Yin, C. Chen, G. a. Krein, C. D. Roberts, J. Segovia, and S.-S. Xu, Phys. Rev. D **100**, 034008 (2019).
[44] P.-L. Yin, Z.-F. Cui, C. D. Roberts, and J. Segovia, Eur. Phys. J. C **81**, 327 (2021).
[45] Y.-Z. Xu, S. Chen, Z.-Q. Yao, D. Binosi, Z.-F. Cui, and C. D. Roberts, Eur. Phys. J. C **81**, 895 (2021).
[46] L. Chang, I. C. Cloët, J. J. Cobos-Martinez, C. D. Roberts, S. M. Schmidt, and P. C. Tandy, Phys. Rev. Lett. **110**, 132001 (2013).
[47] C. Shi, L. Chang, C. D. Roberts, S. M. Schmidt, P. C. Tandy, and H.-S. Zong, Phys. Lett. B **738**, 512 (2014).
[48] C. Shi, C. Chen, L. Chang, C. D. Roberts, S. M. Schmidt, and H.-S. Zong, Phys. Rev. D **92**, 014035 (2015).
[49] K. Raya, Z.-F. Cui, L. Chang, J.-M. Morgado, C. D. Roberts, and J. Rodriguez-Quintero, Chin. Phys. C **46**, 013105 (2022).
[50] C. Shi, K. Bednar, I. C. Cloët, and A. Freese, Phys. Rev. D **101**, 074014 (2020).
[51] J. Carbonell, B. Desplanques, V. A. Karmanov, and J. F. Mathiot, Phys. Rep. **300**, 215 (1998).
[52] X.-d. Ji, J.-P. Ma, and F. Yuan, Phys. Rev. Lett. **90**, 241601 (2003).
[53] S.-x. Qin, L. Chang, Y.-x. Liu, C. D. Roberts, and D. J. Wilson, Phys. Rev. C **85**, 035202 (2012).
[54] C. Shi, M. Li, X. Chen, and W. Jia, Phys. Rev. D **104**, 094016 (2021).
[55] P. A. Zyla *et al.* (Particle Data Group), Prog. Theor. Exp. Phys. **2020**, 083C01 (2020).
[56] C. T. H. Davies, C. McNeile, E. Follana, G. P. Lepage, H. Na, and J. Shigemitsu, Phys. Rev. D **82**, 114504 (2010).
[57] C. McNeile, C. T. H. Davies, E. Follana, K. Hornbostel, and G. P. Lepage, Phys. Rev. D **86**, 074503 (2012).
[58] B. Colquhoun, R. J. Dowdall, C. T. H. Davies, K. Hornbostel, and G. P. Lepage, Phys. Rev. D **91**, 074514 (2015).
[59] J. C. Collins, Acta Phys. Pol. B **34**, 3103 (2003), https://inspirehep.net/files/9e4cfc62067eb5035586fc3e8aea0898.
[60] J. Collins, *Foundations of Perturbative QCD* (Cambridge University Press, Cambridge, England, 2013), Vol. 32.
[61] A. Bacchetta, S. Cotogno, and B. Pasquini, Phys. Lett. B **771**, 546 (2017).
[62] J. C. Collins and D. E. Soper, Nucl. Phys. **B193**, 381 (1981); **B213**, 545(E) (1983).
[63] J. C. Collins, D. E. Soper, and G. F. Sterman, Nucl. Phys. **B250**, 199 (1985).
[64] X.-d. Ji and F. Yuan, Phys. Lett. B **543**, 66 (2002).
[65] X.-d. Ji, J.-p. Ma, and F. Yuan, Phys. Rev. D **71**, 034005 (2005).
[66] J. Lan, C. Mondal, M. Li, Y. Li, S. Tang, X. Zhao, and J. P. Vary, Phys. Rev. D **102**, 014020 (2020).
[67] J. R. Forshaw and R. Sandapen, Phys. Rev. Lett. **109**, 081601 (2012).
[68] J.-h. Yu, B.-W. Xiao, and B.-Q. Ma, J. Phys. G **34**, 1845 (2007).
[69] W. Qian and B.-Q. Ma, Phys. Rev. D **78**, 074002 (2008).
[70] M. A. Ebert, J. K. L. Michel, I. W. Stewart, and Z. Sun, arXiv:2201.07237.
[71] A. Bacchetta and A. Prokudin, Nucl. Phys. **B875**, 536 (2013).
[72] M. G. Echevarria, A. Idilbi, and I. Scimemi, Phys. Rev. D **90**, 014003 (2014).
[73] M. G. Echevarria, T. Kasemets, P. J. Mulders, and C. Pisano, J. High Energy Phys. 07 (2015) 158; 05 (2017) 073(E).
[74] Y. Li, P. Maris, and J. P. Vary, Phys. Rev. D **96**, 016022 (2017).
[75] M. Li, Y. Li, G. Chen, T. Lappi, and J. P. Vary, arXiv:2111.07087.
[76] C. Best, M. Gockeler, R. Horsley, E.-M. Ilgenfritz, H. Perlt, P. E. L. Rakow, A. Schafer, G. Schierholz, A. Schiller, and S. Schramm, Phys. Rev. D **56**, 2743 (1997).
[77] M. Löffler, P. Wein, T. Wurm, S. Weishäupl, D. Jenkins, R. Rödl, A. Schäfer, and L. Walter (RQCD Collaboration), Phys. Rev. D **105**, 014505 (2022).
[78] M. Botje, Comput. Phys. Commun. **182**, 490 (2011).
[79] A. D. Martin, W. J. Stirling, R. S. Thorne, and G. Watt, Eur. Phys. J. C **63**, 189 (2009).
[80] S. J. Brodsky, AIP Conf. Proc. **792**, 977 (2005).
[81] B.-D. Sun and Y.-B. Dong, Phys. Rev. D **96**, 036019 (2017).
[82] L. Mankiewicz, Phys. Rev. D **40**, 255 (1989).
[83] K. D. Bednar, I. C. Cloët, and P. C. Tandy, Phys. Rev. Lett. **124**, 042002 (2020).